Re-Understanding the Reaction Mechanism of Aqueous Zn-Mn Battery in Sulfate Electrolytes: Role of the Zinc Sulfate Hydroxide

Hao Chen, Chunlong Dai, Fangyuan Xiao, Qiuju Yang, Shinan Cai, Maowen Xu, Hong Jin Fan* and Shu-Juan Bao**

H. Chen, F. Xiao, Q. Yang, S. Cai, M. Xu, S.-J. Bao
Institute for Clean Energy & Advanced Materials

School of Materials and Energy

Southwest University

Chongqing 400715, P.R. China
E-mail: xumaowen@swu.edu.cn; baoshj@swu.edu.cn

C. Dai
Beijing Key Laboratory of Photoelectronic/Electrophotonic Conversion Materials,

Key Laboratory of Cluster Science, Ministry of Education

School of Chemistry and Chemical Engineering

Beijing Institute of Technology
Beijing 100081, P. R. China.

H. J. Fan

School of Physical and Mathematical Sciences

Nanyang Technological University

21 Nanyang Link, Singapore 637371, Singapore

E-mail: fanhj@ntu.edu.sg

This article has been accepted for publication and undergone full peer review but has not been through the copyediting, typesetting, pagination and proofreading process, which may lead to differences between this version and the Version of Record. Please cite this article as doi: 10.1002/adma.202109092.

Abstract: Rechargeable aqueous Zn-Mn batteries have garnered extensive attentions for next-generation high-safety energy storage. However, the charge storage chemistry of Zn-Mn batteries remains controversial. Prevailing mechanisms include conversion reaction and cation (de)intercalation in mild acid or neutral electrolytes, and MnO_2/Mn^{2+} dissolution-deposition reaction in strong acidic electrolytes. Herein, we propose a *$Zn_4SO_4{\cdot}(OH)_6{\cdot}xH_2O$ (ZSH) assisted deposition-dissolution model* to elucidate the reaction mechanism and capacity origin in Zn-Mn batteries based on mild acidic sulfate electrolytes. In this new model, the reversible capacity originates from a reversible conversion reaction between ZSH and $Zn_xMnO(OH)_2$ nanosheets; in which the MnO_2 initiates the formation of ZSH but contributes negligibly to the apparent capacity. The role of ZSH in this new model is confirmed by a series of operando characterizations and by constructing Zn batteries using other cathode materials (including ZSH, ZnO, MgO, and CaO). This research may refresh the understanding of the most promising Zn-Mn batteries and guide the design of high-capacity aqueous Zn batteries.

1. Introduction

Rechargeable aqueous Zn-Mn batteries have the advantages of high theoretical capacity, non-toxicity, and low cost of metal zinc and manganese oxide compared to other metal anodes and oxide cathodes.[1] A variety of high energy density and long-term stable aqueous Zn-Mn batteries have been realized, which make them highly promising for application in grid-scale energy storage.[2] In parallel to the progress in the battery performance, the reaction chemistry of the Zn-Mn system has been complex and remains controversial. The energy storage mechanism is intricate due to the variable valences and phases of manganese oxide and the unstable pH value of the electrolyte.[3] Until now, the reported reaction mechanisms of aqueous Zn-Mn batteries in sulfate electrolytes include (1) Zn^{2+} intercalation/de-intercalation or co-intercalation/de-intercalation of Zn^{2+}/H^+ into the MnO_2 lattice;[2a, 4] (2) MnO_2 conversion reaction with H^+;[3c, 5] and (3) MnO_2/Mn^{2+} dissolution-deposition reaction in a strong acidic electrolyte.[6] In particular, the MnO_2/Mn^{2+}dissolution-deposition reaction with a two-electron transfer was first discovered in a Mn-H_2 battery[7] and later was discovered also in Zn-MnO_2 batteries.[6a] This dissolution reaction has been proven by a series of mechanistic studies including *in situ* TEM and *operando* measurements.[8] A unique phenomenon is, $Zn_4SO_4(OH)_6{\cdot}nH_2O$ (ZSH) microsized flakes are generally recognized as a byproduct of side reactions in sulfate electrolytes due to a subtle variation in the local pH value. Recent research proposed that the ZSH based deposition-dissolution reaction can also describe the reaction chemistry of Zn-Mn batteries in the mild acidic sulfate electrolyte, but their conclusions are not consistent with each other.[5a, 9] Hence, the deterministic role of ZSH in aqueous Zn-MnO_2 systems especially its contribution to capacity requires further investigation.

In this work, we challenge the conventional mechanism of aqueous Zn-Mn battery in sulfate-based mild acidic electrolyte and unravel the important role of ZSH. We show that the aqueous Zn-Mn battery in mild acid sulfate electrolytes (pH~4) is more likely driven by a ZSH assisted deposition-dissolution reaction with two electrons transfer, whereas the intercalation contribution can be neglected. In the presence of Mn^{2+} (either contributed by dissolution of solid MnO_2 or from the $MnSO_4$ electrolyte), the ZSH is the reactant and induces the deposition reaction to form layered zinc vernadite ($Zn_xMnO(OH)_2$) nanosheets on the electrode surface during the charge platform around 1.5 V *vs.* Zn/Zn^{2+}. During the discharge, the ZSH re-forms and simultaneously accelerates the proton reaction with $Zn_xMnO(OH)_2$, leading to the dissolution of $Zn_xMnO(OH)_2$ nanosheets. Hence, we propose

that this reversible conversion reaction between ZSH and $Zn_xMnO(OH)_2$ can drives the reversible energy storage reaction of aqueous Zn-Mn batteries.

This model fundamentally differs from the conventional (de)intercalation mechanism or dissolution reaction. In our model, the role of MnO_2 cathode is to promote the initial formation of ZSH by consuming H^+ (i.e., dissolution), but the Mn^{2+} will not back deposit to MnO_2 in subsequent cycles. Interestingly, this model is generic and applicable to a battery system with $MnSO_4$ electrolyte but without MnO_2. This model has been successfully validated in this study by using pure ZSH, ZnO, MgO, and CaO as the cathode materials. The battery performance of these systems depends on the dissolution properties of these materials. We have also identified that the reversibility of the conversion reaction between ZSH and $Zn_xMnO(OH)_2$ is key factor to the cycle stability for sulfate-based aqueous Zn-Mn batteries.

2. Results and Discussion

2.1 Invalidity of conventional (de)intercalation models

To start the experiment, we synthesized the tunneled α-, β-MnO_2 and layered δ-MnO_2 with high-purity (Figure S1, Supporting Information) to re-examine the electrochemical behaviors of the aqueous Zn-Mn battery. As expected, in a 2 M $ZnSO_4$ + 0.5 M $MnSO_4$ electrolyte, similar cyclic voltammetry (CV) and galvanostatic charge-discharge (GCD) curves were observed for the α-MnO_2, β-MnO_2, and δ-MnO_2 cathode materials (**Figure 1** and S2, Supporting Information). As shown in Figure 1A, the α-MnO_2 cathode exhibits two well-separated redox CV peaks (named O1/R1 and O2/R2) at a scan rate of 0.2 mV s^{-1} in the voltage range of 0.8-1.8 V *vs.* Zn^{2+}/Zn. While the CV peak intensities of O1/R1 gradually decrease, those of O2/R2 increase during the initial cycles. The GCD curves for the α-MnO_2 cathode at 200 mA g^{-1} (Figure 1B) present two charge plateaus and discharge plateaus at the second cycle, which are consistent with the CV curves.

To understand the reaction chemistry, the *ex-situ* XRD patterns of α-MnO_2 cathode in 2 M $ZnSO_4$ + 0.5 M $MnSO_4$ electrolyte were collected to examine the possible phase transformation (Figure S3, Supporting Information). It is found that $Zn_4SO_4(OH)_6{\cdot}4H_2O$ (ZSH; PDF # 44-0673) emerges as a new phase after the first discharge process. The ZSH can also be seen from FESEM image (Figure S3C) which shows micron-sized flakes deposited on the electrode surface. In the subsequent charge-discharge process, the *ex-situ* XRD patterns (Figure S4, Supporting Information) reveal good reversibility of ZSH; it

disappears gradually when the battery is charged to 1.54 V *vs.* Zn/Zn^{2+} then re-emerges upon discharging to around 1.30 V *vs.* Zn/Zn^{2+}. In addition, when the 2 M $ZnSO_4$ solution was used as the electrolyte, the same reversible cycle of ZSH was also detected (Figure S5, Supporting Information).

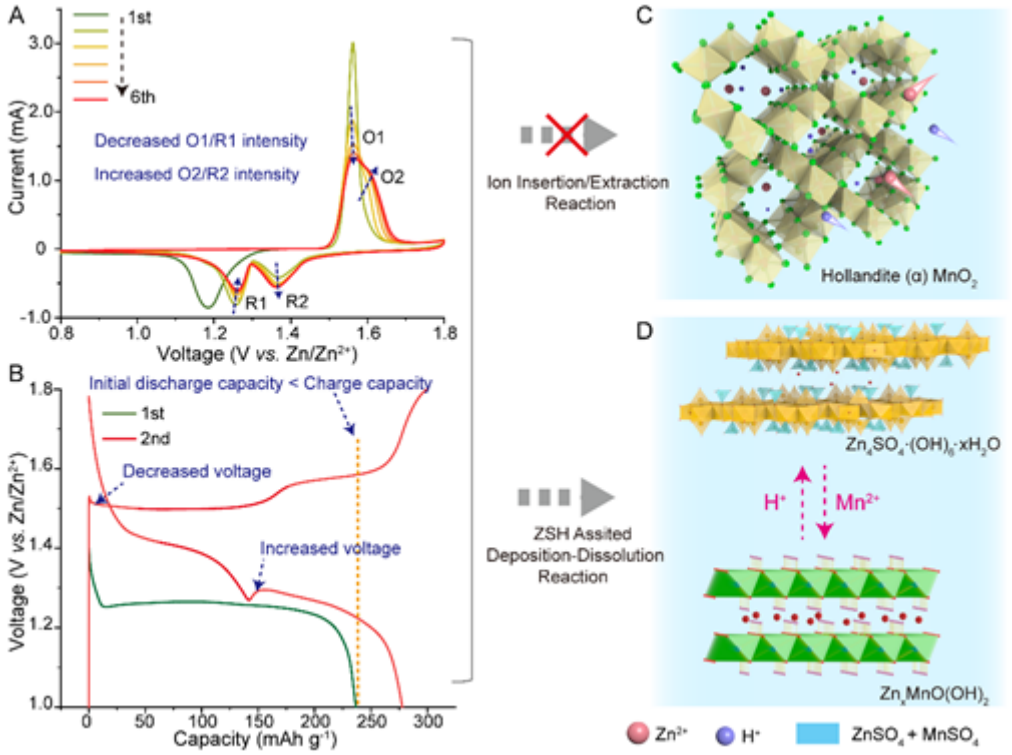

Figure 1. Electrochemistry of Zn/α-MnO_2 battery in a mild acidic sulfate electrolyte (2 M $ZnSO_4$ + 0.5 M $MnSO_4$). (A) Cyclic voltammogram curves at a scan rate of 0.2 mV s^{-1} in the range of 0.8-1.8 V *vs.* Zn/Zn^{2+}. (B) The galvanostatic charge-discharge profiles at 200 mA g^{-1} for the initial two cycles. (C) Schematic of the conventional cation intercalation/de-intercalation reaction model, and (D) Schematic of the ZSH assisted deposition-dissolution conversion reaction model.

More evidence to the role of MnO_2 nanorods during the discharge process is provided by a series of control experiments (see Figure S6-S8 and associated discussions, Supporting Information). This evidence leads to the conclusion that the α-MnO_2 involves in the reaction

only during the first discharge process and contributes little capacity in the subsequent cycles. Hence, the first discharge reaction consumes H^+ and releases Mn^{2+} into the solution according to the following reaction (see also Figure S9, Supporting Information):

$$MnO_2 + 2e^- + 2H^+ \rightarrow Mn^{2+} + 2OH^-$$

This distinguishes itself from the MnO_2/Mn^{2+} dissolution-deposition reaction, in which Mn^{2+} will reversibly redeposit to solid MnO_2.

The reversible ZSH formation-disappearance cycle is consistent with the understanding that the H^+ consumption causes the local pH increase in the electrolyte and the reversible formation and disappearance of ZSH.[3c, 5a, 5b] However, the conventional reaction model based on ion (de)intercalation, which is accompanied by pH-modulated ZSH formation, is invalid to explaining the Zn-Mn battery behavior in the present study. *First*, the O1/R1 redox peak drops and O2/R2 peak rises during the continuous charge/discharge cycles; *Second*, the initial discharge capacity is lower than the subsequent charge capacity; *Last*, the charge voltage exhibits an unusual decrease around 1.5 V *vs.* Zn/Zn^{2+}. Note that the "turning point" around 1.30 V has been related to the deposition of ZHS flakes that results from a local increase in pH.[10]

2.2 New model of ZSH assisted deposition-dissolution

We propose a ZSH assisted deposition-dissolution reaction model to explain the above findings. Under the sulfate-based electrolyte, the aqueous Zn-Mn batteries are driven by a conversion reaction between ZSH and $Zn_xMnO(OH)_2$ during charge and discharge process (schematically shown in Figure 1D), which is accompanied by proton diffusion and a local increase in pH value. In the following, we will provide evidence to the reaction product, $Zn_xMnO(OH)_2$ nanosheets, and prove that this reaction model can well explain the unusual electrochemical phenomena. More interestingly, it can also predict other non-MnO_2 cathode materials for the aqueous Zn/Mn batteries.

As single chemical valence metallic ion compound, $Zn_4SO_4(OH)_6 \cdot 4H_2O$ cannot be used as the host material for reversible cation intercalation/de-intercalation. Hence, the battery must proceed with a different reaction path. To check this, we fabricated a Zn-ZSH battery (i.e., absence of MnO_2) using synthesized ZSH flakes (Figure S10, Supporting Information) as the cathode, metallic Zn as the anode, and 2 M $ZnSO_4$ + 0.5 M $MnSO_4$ as the electrolyte (see

battery architecture in **Figure 2**A). The Zn-ZSH battery exhibits two well-separated redox peaks in the CV curves (Figure 2B) that is similar to the Zn/α-MnO_2 battery. No redox peaks were detected without the Mn^{2+} electrolyte additive (inset of Figure 2B), which suggests that the reversible redox reaction of the Zn-ZSH battery involves electron transfer with Mn^{2+}. These features can also be seen from the GCD curves (Figure 2C), where two charge and discharge plateaus are observed with a discharge specific capacity around 110 mAh g^{-1}. Interestingly, the Zn-ZSH battery displays two charge plateaus without the necessity of an initial discharge process, which is in sharp contrast to the aqueous Zn-MnO_2 battery for which an initial discharge process is mandatory for the reversible energy storage process (Figure S11, Supporting Information).

The phase evolution of the ZSH cathode was characterized during the charge-discharge process. In the *operando* XRD pattern (Figure 2D), in addition to the reflection of the reaction cell used for *operando* measurement (22.0° and 43.9°) and carbon cloth current collector (24.0° and 44.8°), the reflections of ZSH (PDF # 44-0673) exhibit reversible evolution during the charge-discharge process. Further, the ZSH phase weakens gradually during the first charge platform around 1.5 V *vs.* Zn/Zn^{2+}, then totally vanishes when charged to around 1.54 V *vs.* Zn/Zn^{2+}, and re-appear gradually when discharged to around 1.30 V *vs.* Zn/Zn^{2+}. Obviously, the phase evolution process is nearly the same as that of the Zn-MnO_2 battery (Figure S4, Supporting Information). The similarity in battery properties (CV, GCD, and capacity) implies a similar electrochemical behavior in the Zn-ZSH and Zn-MnO_2 batteries when they operate in same electrolyte.

Considering the limited information provided by XRD patterns, *operando* Raman spectra were acquired to investigate the ZSH cathode evolution process. As shown in Figure 2E, the bands around 450 cm^{-1} and 615 cm^{-1} are associated with the stretching vibration (S-O) of the SO_4^{2-} group from the electrolyte.[11] During the charging of the ZSH cathode, three obvious Raman bands around 502, 572, and 676 cm^{-1} emerge gradually, which correspond to the V_4 (Mn-O) stretching vibration mode, stretching vibration of V_3(Mn-O) in the basal plane of [MnO6] sheets that is evident in layered manganese oxides, and symmetric stretching vibration of V_2 (Mn-O) in MnO_6 that is ascribed to the A_{1g} symmetric mode.[12] Consequently, a layered manganese oxide phase emerges gradually during the first charge platform around 1.50 V *vs.* Zn/Zn^{2+}. When the ZSH cathode was discharged, the Raman band of layered manganese oxide weakens gradually then vanishes during the second discharge platform around 1.30 V *vs.* Zn/Zn^{2+}. Hence, *operando* Raman spectroscopy revealed a reversible cycle of layered manganese oxide during the charge-discharge process. The *ex-situ*

X-ray photoelectron spectroscopy (XPS) Mn 2p spectra (Figure 2F) further confirm this evolution process.

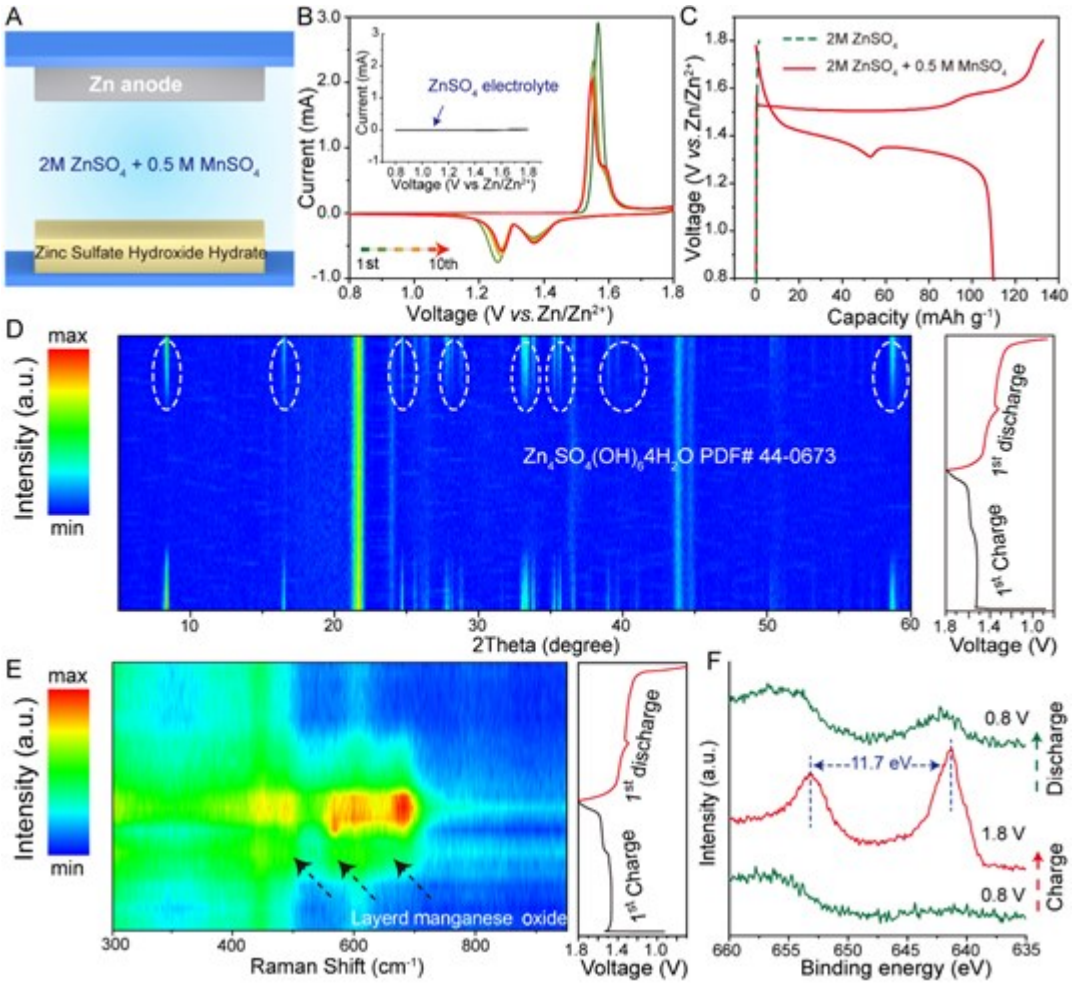

Figure 2. Zn battery based on ZSH cathode material (Zn/ZSH battery). (A) Schematic representation of the Zn-ZSH battery. (B) Cyclic voltammogram curves of Zn-ZSH battery at a scan rate of 0.2 mV s^{-1} from 0.8 -1.8 V *vs.* Zn/Zn^{2+}; inset is the CV curves when using pure $ZnSO_4$ electrolyte. (C) Galvanostatic charge-discharge curves of Zn-ZSH battery at 200 mA g^{-1} in the different electrolytes. (D) *Operando* XRD patterns and (E) *operando* Raman spectra of ZSH electrode during the charge-discharge process at the current density of 200 mA g^{-1}. The dashed circles indicate the peaks from ZSH. (F) *ex-situ* XPS Mn 2p spectra of ZSH electrode at the current density of 200 mA g^{-1}.

In order to further investigate the reversible cycles of ZSH and layered manganese oxide, *ex-situ* FESEM images of the ZSH cathode during the charge-discharge process were collected (**Figure 3**A). Compared to the large flakes in the initial state, the ZSH electrode

surface became uniformly covered by nanosheets when charged to 1.54 V *vs.* Zn/Zn^{2+}, and the formed nanosheets grew larger and the large flakes disappeared as the charging progressed. In the subsequent discharging process, the nanosheets faded gradually after discharging to around 1.30 V *vs.* Zn/Zn^{2+} and then fully transformed into ZSH flakes upon discharging to 0.8 V. Hence, the layered manganese oxide with a nanosheet structure and ZSH with the flake structure appear alternatively during the charge-discharge process. A similar phenomenon was also observed in the case of using the α-MnO_2 cathode (Figure S13, Supporting Information). In the STEM-EDS mappings (Figure 3B), the Mn and O elements were homogeneously distributed on the nanosheets.

Next, we investigated the roles played by the ZSH and layered manganese oxide during the deposition-dissolution reactions by assembling a transparent battery equipment **(**Figure 3C). In this configuration, a FTO glass was half-surface deposited with ZSH using an electro-deposition method was used as the cathode, with 2 M $ZnSO_4$ + 0.5 M $MnSO_4$ aqueous solution as the electrolyte and polished Zn foil as the anode. In the initial stage, the deposited ZSH appears white and the bare FTO is transparent. The ZSH region gradually turned to brown with battery charging and finally become dark-brown at 1.6 V *vs.* Zn/Zn^{2+} (Figure 3D). The dark brown gradually faded during the discharge process and turned pale brown at 0.8 V *vs.* Zn/Zn^{2+} (Figure 3E). No change has been observed for the bare FTO during the whole charge-discharge process. The *ex-situ* XRD pattern and FESEM images (Figure S14-16, Supporting Information) further confirm that similar reactions of the aqueous Zn/ZSH battery occurred on the ZSH part of the FTO cathode, whereas there was no reaction on the bare FTO. Therefore, this result corroborates that the ZSH is the driving force for the deposition-dissolution reaction of layered manganese oxide nanosheets, and the dissolution of layered manganese oxide induces the re-formation of ZSH during the second discharge platform (around 1.30 V *vs.* Zn/Zn^{2+}).

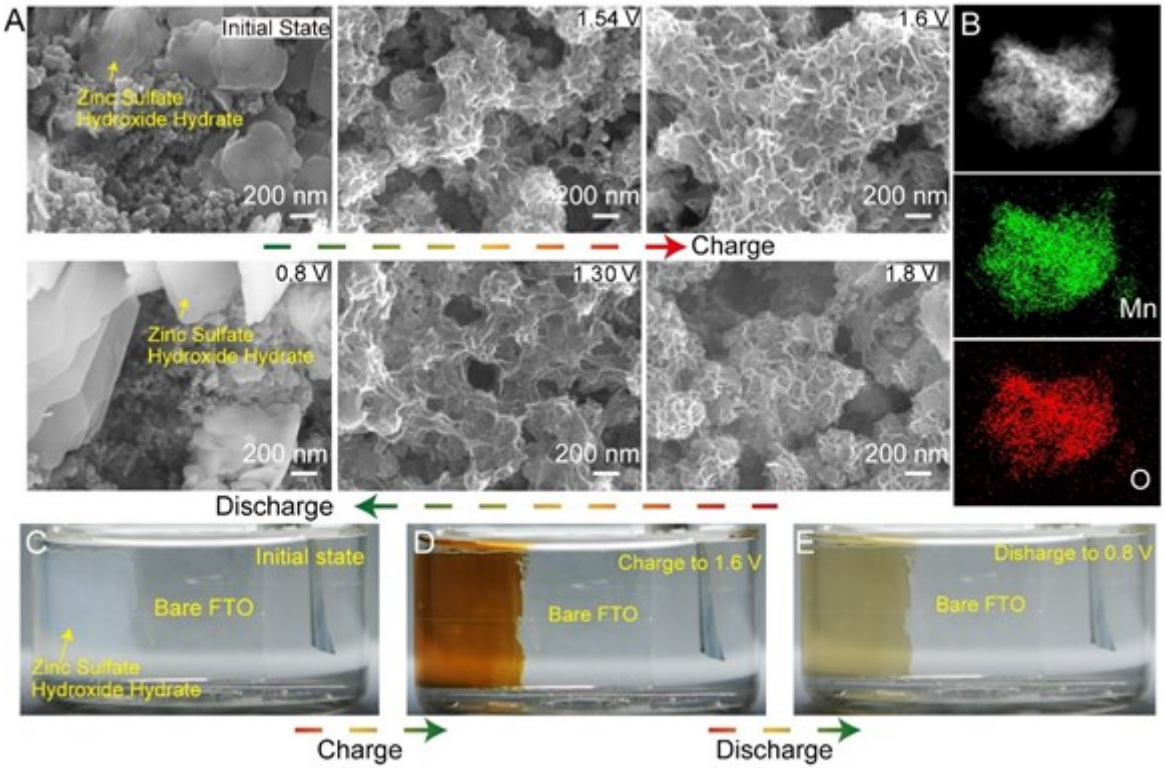

Figure 3. Verification of the reversible deposition-dissolution of ZSH. (A) FESEM images of the ZSH electrode surface at different charge and discharge states in 2 M $ZnSO_4$ + 0.5 M $MnSO_4$ electrolyte. (B) STEM-EDS mapping of the generated nanosheets. (C, D, and E) Digital photos of the transparent Zn-ZSH/FTO battery at different charge and discharge states at 200 mA g^{-1}.

The electron structure and phase of the layered manganese oxide is the key to understanding the reaction chemistry and electron transfer of the aqueous Zn-Mn battery. The TEM images of layered manganese oxide deposited at 1.6 V Zn/Zn^{2+} display a two-dimensional graphene-like structure (**Figure 4**A). The corresponding selected area electron diffraction (inset of Figure 4A) shows a vague diffraction ring, suggesting a low crystallinity that is consistent with the XRD result (Figure 2D). According to the HRTEM image, the interlayer spacing is around 0.47 nm (Figure 4B). Meanwhile, lattice fringes with an inter-planar spacing of 0.24 nm were also observed on the surface of layered MnO_2. To explore the electron structure via *ex-situ* XPS, the Mn 3s spectra were collected from the ZSH cathode (Figure 4C). When charging to 1.54 V *vs.* Zn/Zn^{2+}, the splitting energy (ΔE) between the two Mn 3s peaks was 5.2 eV, which decreases to 4.8 eV with further charging to 1.6 V *vs.*

Zn/Zn^{2+}, then increases to 5.13 eV at the discharge state of 1.30 V *vs.* Zn/Zn^{2+}. Based on the linear relationship between Mn chemical valence and ΔE value of Mn 3s, the average oxidation state of Mn was determined to be 3.34, 3.88, and 3.42 at 1.52, 1.60, and 1.30 V *vs.* Zn/Zn^{2+}, respectively.[13] Moreover, as shown in Figure 4D, the O1s spectra collected from the ZSH cathode can be fitted with two components associated to the Mn-OH bond around 531.7eV and Mn-O-Mn bond around 529.8 eV.[6a] It is obvious that the Mn-O-Mn bond at the charge state of 1.6 V *vs.* Zn/Zn^{2+} is stronger than the previous two.

Based on the analysis of Raman spectra, HRTEM, and XPS results, we suggest that the formed manganese oxide nanosheets are vernadite crystal, a poorly-ordered layered manganese oxide with 4.70 Å theoretical interlayer spacing and a chemical unit of $MnO(OH)_2$.[14] Furthermore, TEM-EDS quantitative analysis (Figure S17, Supporting Information) reveals Zn. Considering a certain amount of Zn^{2+} from electrolyte can go into the manganese oxide interlayers during the deposition process, the deposited nanosheets are zinc vernadite, $Zn_xMnO(OH)_2$.

Hence, the ZSH assisted deposition-dissolution reaction model is proposed as follows (see schematics in Figure 4E). Considering the chemical composition of $Zn_4SO_4{\cdot}(OH)_6{\cdot}4H_2O$, the deposition of ZSH is equivalent to creating a highly basic environment on the electrode surface. From the Nernst equation,[15] the high pH value can reduce the oxidation and deposition potential of Mn^{2+}. Consequently, Mn^{2+} in the basic environment created by ZSH can be oxidized and deposited on the electrode surface at a low charging potential (around 1.5 V *vs.* Zn/Zn^{2+}). Once the ZSH is exhausted, the deposition reaction of Mn^{2+} stops. In other words, Mn^{2+} interacted with ZSH can be oxidized and deposited on the electrode surface during the first charge plateaus (around 1.5 V *vs.* Zn/Zn^{2+}) and then forms into low-crystallinity $Zn_xMnO(OH)_2$ nanosheets via proton-diffusion reaction during the second charge platform (around 1.56 V *vs.* Zn/Zn^{2+}). Subsequently, the $Zn_xMnO(OH)_2$ nanosheets are gradually reduced through the proton-diffusion reaction during the first discharge platform (around 1.43 V *vs.* Zn/Zn^{2+}). With H^+ are consumed, the ZSH will be re-deposited on the electrode surface during the second discharge platform (around 1.30 V *vs.* Zn/Zn^{2+}). The dissolution reaction of $Zn_xMnO(OH)_2$ nanosheets happens when the pH drops locally due to the re-formation of ZSH. The reaction process can be written as follow:

Charge:

$$Zn_4SO_4(OH)_6{\cdot}4H_2O + Mn^{2+} \rightarrow Zn_xMnO(OH)_2 + 4H^+ + SO_4^{2-} + 2e^-$$

Discharge:

$$Zn_xMnO(OH)_2 + 4H^+ + 2e^- \rightarrow Mn^{2+} + Zn^{2+} + 3H_2O$$

$$4Zn^{2+} + SO_4^{2-} + 6OH^- + 4H_2O \rightarrow Zn_4SO_4(OH)_6{\cdot}4H_2O$$

From the chemical valence of Mn and atomic ratio between Mn and Zn of the reaction product $Zn_xMnO(OH)_2$ at 1.6 V vs.Zn/Zn^{2+}, the average chemical formula can be written as $ZnMn_{1.71}O(OH)_{6.63}$. The theoretical discharge capacity of $Zn_xMnO(OH)_2$ is about 175 mAh g^{-1}.

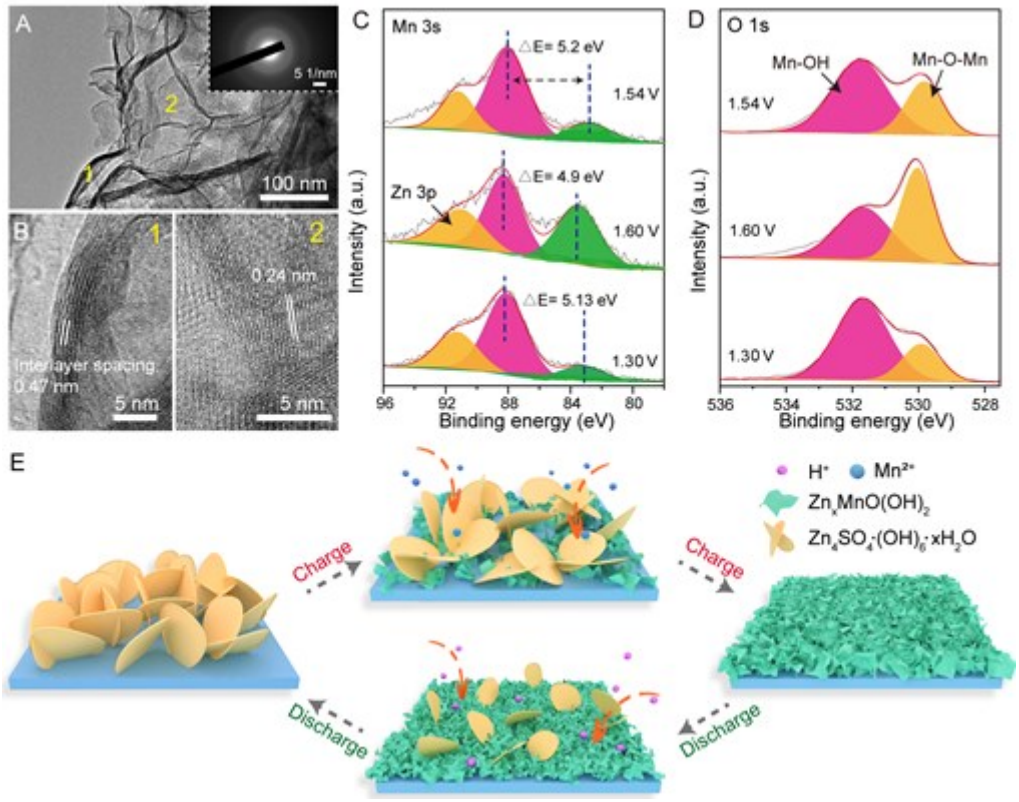

Figure 4. Characterization of the generated layered manganese oxide and its role in Zn-ZSH battery. (A) TEM image of the generated layered manganese oxide at 1.6 V *vs.* Zn/Zn^{2+}, scale bar: 100 nm. Inset is the corresponding selected area electron diffraction (SAED) image, scale bar: 5 1/nm. (B) HRTEM image of generated layered manganese oxide at 1.6 V *vs.* Zn/Zn^{2+}, scale bar: 5 nm. (C and D) High-resolution Mn 3s and O1s XPS spectra of the ZSH electrode at different charge and discharge states. (E) Schematic of the ZSH assisted deposition-dissolution reaction model.

2.3 ZSH assisted deposition-dissolution reaction in other batteries

According to the proposed ZSH assisted deposition-dissolution reaction model, it can be inferred that the same reversible reaction can proceed as long as the cathode material can consume H^+ from the electrolyte. Hence, it is possible to design other cathode materials. We first tested commercial ZnO, a common and low-cost material, as the cathode of a Zn-ZnO battery, using 2 M $ZnSO_4$ + 0.5 M $MnSO_4$ as the electrolyte and Zn foil as the anode (**Figure 5**A). The Zn-ZnO battery exhibits two obvious reversible well-separated redox CV peaks (Figure 5B). The GCD test (Figure 5C) shows that the Zn-ZnO battery can deliver a discharge specific capacity of 230 mAh g^{-1} at 200 mA g^{-1}. The Zn-ZnO battery can retain 60% of its initial capacity after 1000 cycles at a current of 1 A g^{-1} (Figure 5D) and a discharge capacity of 75 mAh g^{-1} at 5 A g^{-1} (Figure 5E). The *operando* XRD pattern, XPS spectra, and SEM images (Figure S18 and S19, Supporting Information) prove the reversible phase evolution of ZSH in the Zn-ZnO battery, which is similar to that of the Zn-MnO_2 and Zn-ZSH batteries.

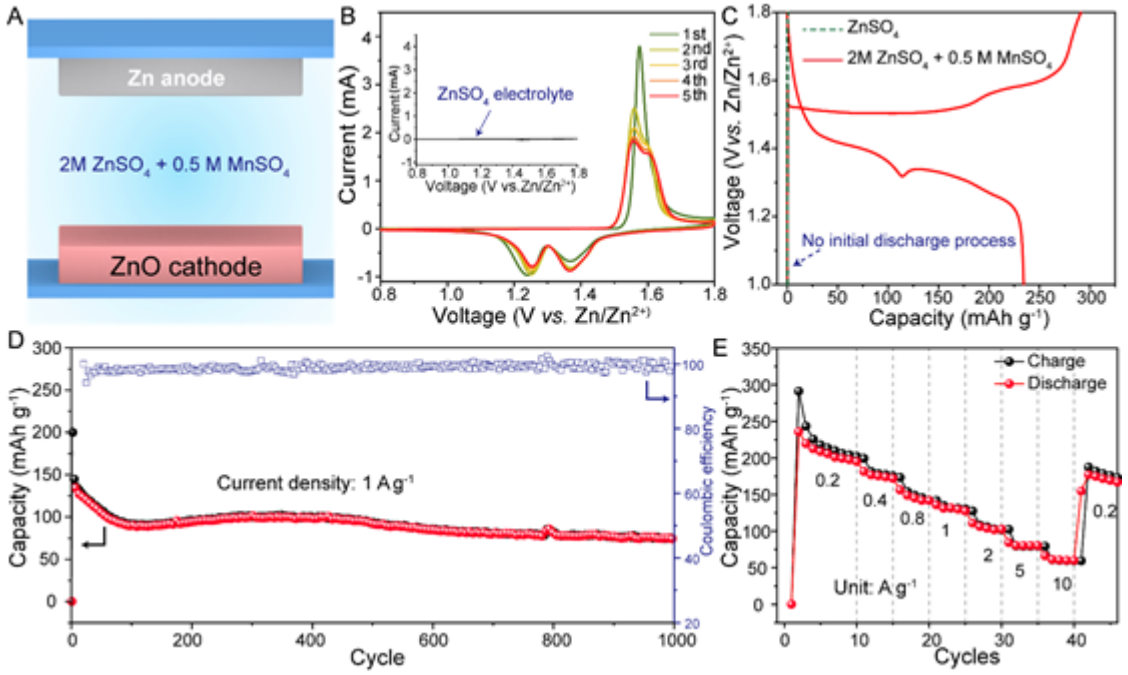

Figure 5. Zn-ZnO battery based on the ZSH assisted deposition-dissolution model. (A) Schematic of the Zn-ZnO battery architecture. (B) Cyclic voltammogram curves at a scan rate of 0.2 mV s^{-1} from 0.8-1.8 V *vs.* Zn/Zn^{2+}; Inset is the CV curves using pure $ZnSO_4$

electrolyte. (C) Galvanostatic charge-discharge curves at 200 mA g^{-1} in different electrolytes. (D) Long-term cycling performance. (E) Rate performance at different current densities.

In order to explore the formation of ZSH in the Zn-ZnO battery system, the ZnO electrode was soaked with 2 M $ZnSO_4$ + 0.5M $MnSO_4$ electrolyte for 2 h. ZSH emerged as a new phase with a large-flake structure on the ZnO electrode surface after the soaking treatment (Figure S20, Supporting Information). Considering the slightly acidic electrolyte, the reaction path for the formation of ZSH is proposed as follows:

$$H_2O \rightarrow H^+ + OH^-$$

$$ZnO + 2H^+ \rightarrow Zn^{2+} + H_2O$$

$$4Zn^{2+} + SO_4^{2-} + 6OH^- + 4H_2O \rightarrow Zn_4SO_4(OH)_6 \cdot 4H_2O$$

Unlike the MnO_2 cathode in which ZSH is deposited during the initial discharge process because of the proton-diffusion reaction, the deposition of ZSH on the ZnO cathode results from the dissolution of ZnO.

In addition to ZnO, we investigated ZSH deposition on a series of other metal oxides, and the results are summarized in **Table 1**. It should be mentioned that the more ZSH exists on the electrode, the more $Zn_xMnO(OH)_2$ nanosheets can be deposited, and consequently, the higher the apparent capacity. When the α-MnO_2 electrode discharged to 0.8 V *vs.* Zn/Zn^{2+}, ZSH of around 1.65 mg was deposited on the electrode surface and around 0.6 mg MnO_2 dissolved. Thus, the α-MnO_2 cathode delivered a reversible specific capacity of around 275 mAh g^{-1} at 200 mA g^{-1} (Figure 1B). However, when the α-MnO_2 electrode was directly immersed in the electrolyte without an initial discharging action, no ZSH phase was detected on the electrode surface, indicating no charge reaction. Comparatively, the ZnO cathode achieves a discharge specific capacity of 230 mAh g^{-1} at 200 mA g^{-1} (Figure 5E). For the CuO or TiO_2 electrodes, their mass remained unchanged after the soaking treatment and no new phase can be detected (Figure S21, Supporting Information). However, the MgO and CaO electrode dramatically changed after soaking treatment, and ZSH deposition was detected as a new phase on both electrodes (Figure S22 and S23, Supporting Information).

Therefore, we suggest that MgO and CaO can also be used as the cathode materials for aqueous batteries (see below).

Table 1. Various metal oxides electrode materials treated in 2 M $ZnSO_4$ + 0.5 M $MnSO_4$ electrolyte for 2 hours at room temperature.

Cathode material	Treatment method	Initial electrode mass[a] (active material mass)	Electrode mass after treatment	Dissolved metal ion	Deposited new products after treatment (mass)
α-MnO_2	Discharge to 0.8 V	1.29 mg (0.90 mg)	2.32 mg	0.39 mg (Mn^{2+})	ZSH (1.65 mg)
	Soaked in the electrolyte[b]	1.68 mg (1.17 mg)	1.72 mg	0.052 mg (Mn^{2+})	No
ZnO	Soaked in the electrolyte	2.22 mg (1.55 mg)	3.21 mg	--[c]	ZSH (--)
MgO	Soaked in the electrolyte	1.89 mg (1.32 mg)	3.56 mg	0.56 mg (Mg^{2+})	ZSH (2.6 mg)
CaO	Soaked in the electrolyte	1.74 mg (1.22 mg)	3.40 mg	0.081 mg (Ca^{2+})	ZSH/$CaSO_4 \cdot 2H_2O$ (1.77 mg)
TiO_2	Soaked in the electrolyte	2.03 mg (1.42 mg)	2.04 mg	0.010 mg (Ti^{4+})	No
CuO	Soaked in the electrolyte	2.43 mg (1.70 mg)	2.42 mg	0.013 mg (Cu^{2+})	No

Note: [a] The mass of the current collector has been deducted, and the electrode area is around 1.3 cm^2. [b] To determine the dissolved mass of Mn^{2+}, the α-MnO_2 electrode was treated in a 2 M $ZnSO_4$ solution which has a similar pH value to that of 2 M $ZnSO_4$ + 0.5 M $MnSO_4$ solution (4.3 vs 3.9). [c] The mass of ZSH deposited on the ZnO electrode cannot be calculated because it is challenge to determine accurately the mass of dissolved Zn^{2+} in the electrolyte. Data of mass is averaged from 3 measurements where the differences are <1%.

Both the MgO and CaO cathodes exhibit well-defined redox CV peaks at a sweeping rate of 0.2 mV s^{-1} between 0.8-1.8 V *vs.* Zn/Zn^{2+} in the 2 M $ZnSO_4$ + 0.5 M $MnSO_4$ electrolyte (Figure S24C and F, Supporting Information). In comparison, when pure 2 M $ZnSO_4$ or pure 0.5 M $MnSO_4$ solution is used as the electrolyte, no obvious redox reaction can be detected from the MgO and CaO cathodes (Figure S24, Supporting Information). This is in accordance

to our model that, for MgO and CaO, Zn^{2+} is needed to provide the source for ZSH formation and Mn^{2+} is required for the redox reaction between ZSH and $Zn_xMnO(OH)_2$. The MgO and CaO cathode exhibit similar GCD curves to the Zn/MnO_2 battery (**Figure 6**A). In the initial charge process, the MgO cathode delivered a high specific capacity of 525 mAh g^{-1} at 200 mA g^{-1} due to the high quantity of ZSH deposition (**Table 1**). For the CaO cathode, the relatively low specific capacity is consistent with the small deposition mass of ZSH. The *ex*-situ XRD pattern reveals reversibility of ZSH on both MgO and CaO cathodes during the charge-discharge process (Figure S25 and S26, Supporting Information). For the rate performance (Figure 6B), the Zn-CaO battery is inferior to the MgO cathode at varying current densities, which can be ascribed to the higher deposition quantity of ZSH on the MgO cathode than that on CaO. And the capacity retention of the Zn-CaO battery is evidently better than the Zn/MgO battery (Figure 6C), which could be related to the deposition of stable $CaSO_4 \cdot 2H_2O$ phase on the CaO cathode (Figure S26, Supporting Information).[16]

To better evaluate the specific capacity, the Zn-ZnO, Zn-MgO and Zn-CaO batteries are compared with the reported Zn-MnO_2 batteries containing Mn^{2+} electrolyte additive (Figure 6C). Similar to ZnO and CaO, the MnO_2 cathode generally deliver a specific capacity around 250 mAh g^{-1} at 200 mA g^{-1}. However, the MgO cathode battery exhibits a more superior discharge specific capacity of 422 mAh g^{-1} at 200 mA g^{-1}. In a nutshell, we believe there are other cathode materials that can be employed for aqueous Zn-Mn batteries based on the ZHS-assisted deposition-dissolution chemistry.

Finally, we emphasize that the basic condition to realize the ZSH based deposition-dissolution model is that Mn^{2+} must be available, either from the cathode material (MnO_2) or from the electrolytes (Table S2, Supporting Information). However, to achieve good battery performance, one needs to optimize the composite electrolyte (concentration and pH) and the anode. For example, for all the cathode materials we investigated herein, the solution of 2 M $ZnSO_4$ + 0.5 M $MnSO_4$ is recommended.

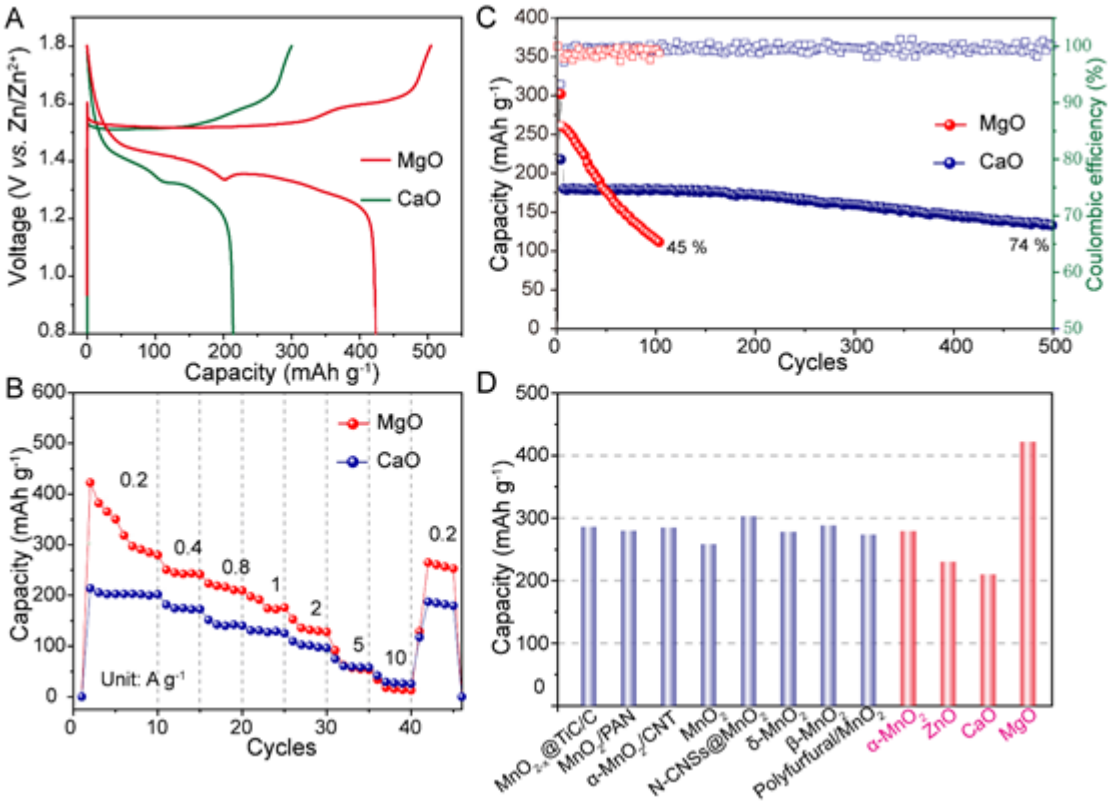

Figure 6. Zn/MgO and Zn/CaO batteries based on the ZSH assisted deposition-dissolution model. (A) Initial Galvanostatic charge-discharge curves of the batteries between 0.8-1.8 V *vs.* Zn/Zn^{2+} at 200 mA g^{-1}. (B) Rate performance at different current densities. (C) Cycling performance between 0.8-1.8 V *vs.* Zn/Zn^{2+} at 500 mA g^{-1}. (D) The comparison of specific capacity between the proposed battery in this work and the recently reported data about various Zn/MnO_2 battery containing Mn^{2+} electrolyte additive at 200 mA g^{-1}, including Zn/MnO_{2-x}@TiC/C,[17] Zn/MnO_2/PAN,[2a] Zn/α-MnO_2/CNT,[18] Zn/MnO_2,[19] Zn/N-CNSs@MnO_2,[20] Zn/δ-MnO_2,[21] Zn/β-MnO_2[22] and Zn/Polyfurfural/MnO_2 battery[23].

3. Conclusion

A ZSH assisted deposition-dissolution reaction model can successfully explain the electrochemical process of aqueous Zn-MnO_2 batteries in sulfate-based electrolytes. When MnO_2 is used as the cathode material, its function is to promote the deposition of $Zn_4SO_4{\cdot}(OH)_6{\cdot}xH_2O$ (ZSH) and release Mn^{2+} into the electrolyte in the first discharge process, while the capacity in subsequent cycles is predominantly contributed by the reversible conversion reaction between ZSH and layered $Zn_xMnO(OH)_2$ nanosheets. This

dynamic conversion reaction is modulated by local pH variations. Our model may be generic to aqueous batteries involving Zn^{2+} and Mn^{2+} either in the form of cathode material or sulfate electrolyte. Based on this new model, we have achieved proof-of-concept demonstration of Zn batteries using other non-MnO_2 cathode materials, including pure ZSH, ZnO, MgO, and CaO. It is suggested that improving the reversibility of the conversion reaction between ZSH and layered $Zn_xMnO(OH)_2$ nanosheets is essential to the stability of the batteries. This model applies to the mild acidic (pH ~ 4) sulfate electrolyte solution and may not contradict to the dissolution-deposition reaction of Mn^{2+} in strong acidic solutions.

Supporting Information

Supporting Information is available from the Wiley Online Library or from the author.

Acknowledgements

This work is financially supported by the National Natural Science Foundation of China (21972111, 21773188), Natural Science Foundation of Chongqing (cstc2018jcyjAX0714), and Venture & Innovation Support Program for Chongqing Overseas Returnees (cx2019073), Chongqing Engineering Research Center for Micro-Nano Biomedical Materials and Devices, and Chongqing Key Laboratory for Advanced Materials and Technologies. H.J.F. thanks the financial support from MOE by Tier 1 grant (RG 85/20).

Conflict of Interest

The authors declare no conflict of interest.

Keywords: Aqueous Zn-Mn battery; Zn-ion battery; conversion reaction; ZSH assisted deposition-dissolution; ZnO battery

Received: ((will be filled in by the editorial staff))
Revised: ((will be filled in by the editorial staff))
Published online: ((will be filled in by the editorial staff))

References:

[1] a) M. Song, H. Tan, D. Chao, H. J. Fan, *Adv. Funct. Mater.* **2018**, 28, 1802564; b) G. Fang, J. Zhou, A. Pan, S. Liang, *ACS Energy Lett.* **2018**, 3, 2480; c) X. Liu, J. Yi, K. Wu, Y. Jiang, Y. Liu, B. Zhao, W. Li, J. Zhang, *Nanotechnology* **2020**, 31, 122001; d) A. Konarov, N. Voronina, J. H. Jo, Z. Bakenov, Y.-K. Sun, S.-T. Myung, *ACS Energy Lett.* **2018**, 3, 2620; e) L. E. Blanc, D. Kundu, L. F. Nazar, *Joule* **2020**, 4, 771; f) X. Jia, C. Liu, Z. G. Neale, J. Yang, G. Cao, *Chem. Rev.* **2020**, 120, 7795.

[2] a) J. Huang, Z. Wang, M. Hou, X. Dong, Y. Liu, Y. Wang, Y. Xia, *Nat. Commun.* **2018**, 9, 1; b) J. Huang, X. Tang, K. Liu, G. Fang, Z. He, Z. Li, *Mater. Today Energy* **2020**, 17, 100475; c) B. Wu, G. Zhang, M. Yan, T. Xiong, P. He, L. He, X. Xu, L. Mai, *Small* **2018**, 14, 1703850; d) H. Chen, H. Kuang, F. Liu, Y. Wu, S. Cai, M. Xu, S.-J. Bao, *J. Colloid Interface Sci.* **2021**, 600, 83; e) M. Chamoun, W. R. Brant, C.-W. Tai, G. Karlsson, D. Noréus, *Energy Storage Mater.* **2018**, 15, 351.

[3] a) M. H. Alfaruqi, V. Mathew, J. Gim, S. Kim, J. Song, J. P. Baboo, S. H. Choi, J. Kim, *Chem. Mater.* **2015**, 27, 3609; b) B. Lee, H. R. Seo, H. R. Lee, C. S. Yoon, J. H. Kim, K. Y. Chung, B. W. Cho, S. H. Oh, *ChemSusChem* **2016**, 9, 2948; c) W. Liu, X. Zhang, Y. Huang, B. Jiang, Z. Chang, C. Xu, F. Kang, *J. Energy Chem.* **2021**, 56, 365.

[4] W. Sun, F. Wang, S. Hou, C. Yang, X. Fan, Z. Ma, T. Gao, F. Han, R. Hu, M. Zhu, *J. Am. Chem. Soc.* **2017**, 139, 9775.

[5] a) H. Pan, Y. Shao, P. Yan, Y. Cheng, K. S. Han, Z. Nie, C. Wang, J. Yang, X. Li, P. Bhattacharya, *Nature Energy* **2016**, 1, 1; b) X. Gao, H. Wu, W. Li, Y. Tian, Y. Zhang, H. Wu, L. Yang, G. Zou, H. Hou, X. Ji, *Small* **2020**, 16, 1905842; c) Q. Zhao, X. Chen, Z. Wang, L. Yang, R. Qin, J. Yang, Y. Song, S. Ding, M. Weng, W. Huang, J. Liu, W. Zhao, G. Qian, K. Yang, Y. Cui, H. Chen, F. Pan, *Small* **2019**, 15, 1904545.

[6] a) D. Chao, W. Zhou, C. Ye, Q. Zhang, Y. Chen, L. Gu, K. Davey, S. Z. Qiao, *Angew. Chem. Int. Ed.* **2019**, 58, 7823; b) M. Wang, X. Zheng, X. Zhang, D. Chao, S. Z. Qiao, H. N. Alshareef, Y. Cui, W. Chen, *Adv. Energy Mater.* **2021**, 11, 2002904; c) C. Zhong, B. Liu, J. Ding, X. Liu, Y. Zhong, Y. Li, C. Sun, X. Han, Y. Deng, N. Zhao, *Nature Energy* **2020**, 5, 440; d) T. Xue, H. J. Fan, *J. Energy Chem.* **2020**, 54, 194.

[7] W. Chen, G. Li, A. Pei, Y. Li, L. Liao, H. Wang, J. Wan, Z. Liang, G. Chen, H. Zhang, J. Wang, Y. Cui, *Nature Energy* **2018**, 3, 428.

[8] a) O. Fitz, C. Bischoff, M. Bauer, H. Gentischer, K. P. Birke, H.-M. Henning, D. Biro, *ChemElectroChem* **2021**, 8, 3553; b) D. Wu, L. M. Housel, S. J. Kim, N. Sadique, C. D. Quilty, L. Wu, R. Tappero, S. L. Nicholas, S. Ehrlich, Y. Zhu, *Energy Environ. Sci.* **2020**, 13, 4322; c) S. J. Kim, D. Wu, N. Sadique, C. D. Quilty, L. Wu, A. C. Marschilok, K. J. Takeuchi, E. S. Takeuchi, Y. Zhu, *Small* **2020**, 16, 2005406.

[9] a) H. Chen, S. Cai, Y. Wu, W. Wang, M. Xu, S.-J. Bao, *Mater. Today Energy* **2021**, 20, 100646; b) X. Guo, J. Zhou, C. Bai, X. Li, G. Fang, S. Liang, *Mater. Today Energy* **2020**, 16, 100396.

[10] a) G. Fang, C. Zhu, M. Chen, J. Zhou, B. Tang, X. Cao, X. Zheng, A. Pan, S. Liang, *Adv. Funct. Mater.* **2019**, 29, 1808375; b) J. Wang, J.-G. Wang, H. Liu, C. Wei, F. Kang, *J. Mater. Chem. A* **2019**, 7, 13727.

[11] X. Guo, H.-S. Xiao, F. Wang, Y.-H. Zhang, *J. Phys. Chem. A* **2010**, 114, 6480.

[12] a) C. Julien, M. Massot, R. Baddour-Hadjean, S. Franger, S. Bach, J. Pereira-Ramos, *Solid State Ionics* **2003**, 159, 345; b) C. Julien, M. Massot, *Phys. Chem. Chem. Phys.* **2002**, 4, 4226.

[13] a) M. C. Biesinger, B. P. Payne, A. P. Grosvenor, L. W. Lau, A. R. Gerson, R. S. C. Smart, *Appl. Surf. Sci.* **2011**, 257, 2717; b) M. Chigane, M. Ishikawa, *J. Electrochem. Soc.* **2000**, 147, 2246.

[14] a) F. Chukhrov, A. Gorshkov, E. Rudnitskaya, V. Beresovskaya, A. Sivtsov, *Clays Clay Miner.* **1980**, 28, 346; b) S. Grangeon, F. Warmont, C. Tournassat, B. Lanson, M. Lanson, E. Elkaïm, F. Claret, *Eur. J. Mineral.* **2017**, 29, 767.

[15] M. M. Walczak, D. A. Dryer, D. D. Jacobson, M. G. Foss, N. T. Flynn, *J. Chem. Educ.* **1997**, 74, 1195.

[16] S. Guo, S. Liang, B. Zhang, G. Fang, D. Ma, J. Zhou, *ACS Nano* **2019**, 13, 13456.

[17] Y. Zhang, S. Deng, M. Luo, G. Pan, Y. Zeng, X. Lu, C. Ai, Q. Liu, Q. Xiong, X. Wang, *Small* **2019**, 15, 1905452.

[18] Y. Liu, X. Chi, Q. Han, Y. Du, J. Huang, Y. Liu, J. Yang, *J. Power Sources* **2019**, 443, 227244.

[19] N. Zhang, F. Cheng, J. Liu, L. Wang, X. Long, X. Liu, F. Li, J. Chen, *Nat. Commun.* **2017**, 8, 1.

[20] Y. Zhang, S. Deng, Y. Li, B. Liu, G. Pan, Q. Liu, X. Wang, X. Xia, J. Tu, *Energy Storage Mater.* **2020**, 29, 52.

[21] D. Wang, L. Wang, G. Liang, H. Li, Z. Liu, Z. Tang, J. Liang, C. Zhi, *ACS Nano* **2019**, 13, 10643.

[22] M. Liu, Q. Zhao, H. Liu, J. Yang, X. Chen, L. Yang, Y. Cui, W. Huang, W. Zhao, A. Song, *Nano Energy* **2019**, 64, 103942.

[23] Q. Zhao, X. Huang, M. Zhou, Z. Ju, X. Sun, Y. Sun, Z. Huang, H. Li, T. Ma, *ACS Appl. Mater. Interfaces* **2020**, 12, 36072.

Table of Contents Entry

A new ZSH assisted deposition and dissolution reaction model has been proposed and validated for aqueous Zn-Mn batteries in mild sulfate electrolytes. We show that MnO_2 is not a compulsory cathode; and various metal oxides, including ZSH, ZnO, MgO and CaO, can be used as the cathode materials for aqueous Zn batteries.